

ARTICLE OPEN



Strain derivative of thermoelectric properties as a sensitive probe for nematicity

F. Caglieris^{1,2}✉, C. Wuttke¹, X. C. Hong¹, S. Sykora¹, R. Kappenberger¹, S. Aswartham¹, S. Wurmehl¹, B. Büchner^{1,3,4} and C. Hess^{1,4,5}

The nematic instability is an undebatable ingredient of the physics of iron-based superconductors. Yet, its origin remains enigmatic as it involves a fermiology with an intricate interplay of lattice-, orbital-, and spin degrees of freedom. It is well known that thermoelectric transport is an excellent probe for revealing even subtle signatures of instabilities and pertinent fluctuations. In this paper, we report a strong response of the thermoelectric transport properties of two underdoped 1111 iron-based superconductors to a vanishingly small strain. By introducing the strain derivative of the Seebeck and the Nernst coefficients, we provide a description of the nematic order parameter, proving the existence of an anisotropic Peltier-tensor beside an anisotropic conductivity tensor. Our measurements reveal that the transport nematic phenomenology is the result of the combined effect of both an anisotropic scattering time and Fermi surface distortions, pointing out that in a realistic description, abreast of the spin fluctuations also the orbital character is a fundamental ingredient. In addition, we show that nematic fluctuations universally relax in a Curie–Weiss fashion above T_S in all the elasto-transport measurements and we provide evidences that nematicity must be band selective.

npj Quantum Materials (2021)6:27; <https://doi.org/10.1038/s41535-021-00324-7>

INTRODUCTION

The investigation of nematic orders in solid-state systems has been strongly boosted in recent times by the hypothesis of their intimate link with the emerging unconventional superconductivity in copper-based^{1,2} and specially in iron-based superconductors^{3,4}. In the latter, the nematic order identifies a lowering of the rotational symmetry characterized by a tetragonal-to-orthorhombic structural transition, which typically anticipates the formation of a magnetic order with additional signatures of orbital ordering^{3,4}. This crossover of multiple orders generate a "chicken-or-egg" problem, whose solution is considered a crucial step towards the understanding of the unconventional superconductivity³.

One of the most successful experimental approach to this dilemma is the study of the strain susceptibility of different physical quantities in proximity of the structural transition. Remarkably, the use of the strain derivative of the electrical resistivity as a sensitive quantity mimic of the nematic susceptibility allowed to track the evolution of the nematic fluctuations and to distinguish their electronic origin from a simple ferroelastic distortion^{5–7}. Although this promotes the nematic order to the same level of the other electronic instabilities (i.e., superconductivity and density waves), its microscopic origin remains a puzzle, in particular concerning the role of the orbital and spin degrees of freedom. It is common wisdom that thermoelectric transport properties are excellent probes to investigate the fermiology of unconventional materials. In the vicinity of electronic instabilities, they could exhibit spectacular effects, resulting in an extreme sensitivity to phase transitions and fluctuations of order parameters^{8–12}. Therefore, in proximity of an electronic nematic instability, the evaluation of the thermoelectric response to an applied uniaxial strain, appears as

an ideal experimental approach to unveil the role of Fermi Surface distortions.

In this regard, particularly promising is the observation of a strong anisotropy in the Seebeck (S) and the Nernst (ν) coefficients in the nematic phase of some detwinned 122 iron-based superconductors^{13–16}, as a direct indication of a possible strong elasto-thermoelectric effect. In order to exploit this potential, we introduce the elasto-Seebeck effect and the elasto-Nernst effect, defined as the strain derivative of S and ν in the limit of vanishingly small strain ϵ . Experimentally, we take advantage of an innovative setup, which combines a standard thermoelectric measurement configuration, with the highly controlled uniaxial strain offered by a piezoelectric device. By measuring directly the slope of S and ν vs ϵ , we have access to the respective strain derivatives (Fig. 1, see Materials and Methods for details on the experimental setup), representing the nematic susceptibility of the system. In particular, in this work, we investigate the transport nematic phenomenology of two single crystals of $\text{LaFe}_{1-x}\text{Co}_x\text{AsO}$ with $x = 0$ and 0.035 ^{17,18}, respectively. The former is the parent compound and the latter an electron underdoped sample of the La-1111 family, so far almost unexplored due to the lack of sizeable single crystals.

We will show that the thermoelectric transport properties react extraordinarily to a tiny strain well above the nematic transition, revealing an extended zone of nematic fluctuations with a diverging behavior at the structural transition. Moreover, by analyzing the contribution of the different transport coefficients we demonstrate that a band-selective response of the Peltier-tensor α is indispensable to quantitatively explain the behavior of the thermoelectric coefficient under strain, pointing out the fundamental role of the Fermi surface distortions caused by electron-nematic order¹⁹. In addition, we experimentally

¹Leibniz-Institute for Solid State and Materials Research, Dresden, Germany. ²CNR-SPIN, Genova, Italy. ³Institut für Festkörperphysik, TU Dresden, Dresden, Germany. ⁴Center for Transport and Devices, TU Dresden, Dresden, Germany. ⁵Fakultät für Mathematik und Naturwissenschaften, Bergische Universität Wuppertal, Wuppertal, Germany. ✉email: federico.caglieris@spin.cnr.it

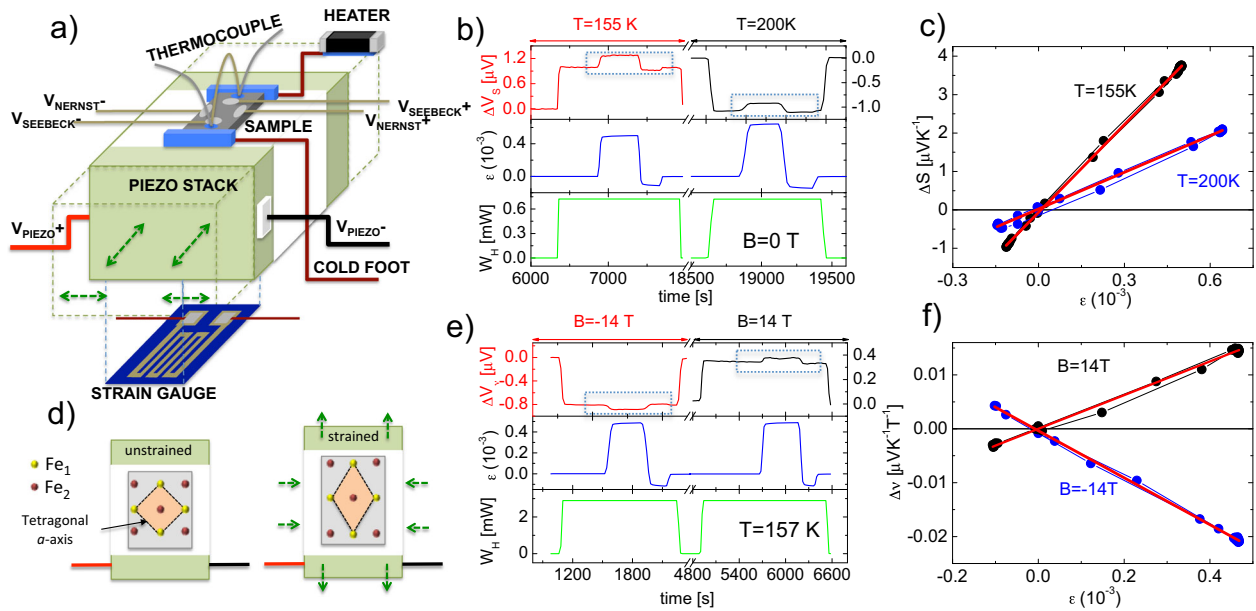


Fig. 1 The elasto-thermoelectric transport technique. **a** Schematic of our experimental setup. The relative size of the sample and the piezo-stack in the sketch is exaggerated: the actual size of the piezo device is $9 \times 5 \times 5 \text{ mm}^3$, while the sample is around $1 \times 1 \times 0.04 \text{ mm}^3$. The sample is mounted on a piezoelectric device, which expands or contracts according to the green arrows. The thermal circuit is realized with a heater and a cold foot connected to the thermal mass. The temperature gradient is measured using a chromel-Au thermocouple while two couples of electrodes measure the Seebeck voltage ΔV_S and the Nernst voltage ΔV_N . The applied strain ϵ is measured with a strain gauge glued on the back side of the piezo. **d** The sample is oriented with the tetragonal a -axis tilted of 45 degrees with respect to the piezo straining axis, so that the distortion occurs along the putative orthorhombic axis. Fe_1 and Fe_2 are the iron atoms in the Fe-As planes. **b, e** Time-dependence of the applied heat power W_H (bottom panel), applied strain ϵ (middle panel) and resulting Seebeck (**b**) and Nernst (**e**) signals at representative temperatures and magnetic fields for a LaFeAsO compound. **c** Strain dependence of the Seebeck anisotropy $\Delta S = S(\epsilon) - S(\epsilon = 0)$ for a single crystal of LaFeAsO at $T = 155 \text{ K}$ and $T = 200 \text{ K}$. **f** Strain dependence of the Nernst anisotropy $\Delta \nu = \nu(\epsilon) - \nu(\epsilon = 0)$ for a single crystal of LaFeAsO at $T = 157 \text{ K}$ and $B = \pm 14 \text{ T}$.

demonstrate that, within the validity of a single-band approximation, the elasto-Nernst coefficient can be predicted as a combination of the strain derivatives of the Peltier α and the conductivity σ tensors. This lets us paint a self-consistent scenario in which all the elasto-transport coefficients are bound to each other.

RESULTS

Elasto-Seebeck

Figure 2a, b shows the temperature dependence of Seebeck coefficient S of the $x = 0$ and the $x = 0.035$ sample, respectively. Their amplitude and trend are consistent with previous reports on polycrystalline compounds⁹. In the $x = 0$ sample a sign change of S occurs at around 170 K, caused by the multiband nature of this material. Since hole-like and electron-like pockets contribute to the Seebeck coefficient with opposite sign, they tend to compensate their respective effect, possibly generating a change in the sign of S , as in our case. In the $x = 0.035$ compound, the electron doping, obtained by Co-substitution, pushes it closer to the condition of single-carrier transport and the Seebeck coefficient remains always negative, as expected for a system dominated by electrons. This has been already shown in La(Fe,Co)AsO and Sm(Fe,Co)AsO series of polycrystalline samples, where a departure from the carrier compensation in favour of an electron-like transport due to Co-doping has been demonstrated^{20,21}.

Figure 2c, d presents the temperature dependence of the strain (ϵ) derivative of the Seebeck coefficient $\delta(\Delta S/T)/\delta\epsilon$, with $\Delta S = S(\epsilon) - S(\epsilon = 0)$, for the $x = 0$ and $x = 0.035$ compound, respectively (the elasto-Seebeck effect of an additional sample with $x = 0.01$ is reported in Supplementary Note 3 and Supplementary Fig. 4). The normalization to T is introduced to get rid of the entropy contribution. Interestingly, in both the compounds a change of

regime appears in correspondence of the structural transition, whose onset is around $T_S = 155 \text{ K}$ in the parent compound and $T_S = 80 \text{ K}$ for the underdoped one¹⁸. While $\delta(\Delta S/T)/\delta\epsilon$ of the $x = 0$ compound exhibits a sharp cusp-like transition, in the $x = 0.035$ compound the change of regime at T_S is more broadened. However, for $T > T_S$, where the crystalline cell is tetragonal and nematic fluctuation are expected, $\delta(\Delta S/T)/\delta\epsilon$ is finite and large in both the compounds, evidencing a strong response of the Seebeck coefficient to a vanishingly small strain. Moreover, $\delta(\Delta S/T)/\delta\epsilon$ exhibits a diverging trend by approaching T_S . This behavior is typically detected in the context of elastoresistivity measurements, where a Curie-Weiss fashion of the elastoresistivity is interpreted as the fingerprint of large nematic fluctuations with an electronic origin^{5,6,22}.

In addition, with our experimental approach we could also take advantage of the fact that S is sensitive to the sign of the charge carriers. Indeed, the most striking result of our measurement concerns the sign of $\delta(\Delta S/T)/\delta\epsilon$: In the parent compound, though S changes sign, $\delta(\Delta S/T)/\delta\epsilon$ is always positive and it remains finite also when S crosses the zero. This points out that not all the different Fermi pockets are responsible for the electronic nematic phenomenology but only some of them contribute. Interestingly, the strain derivative persists to be positive also in the $x = 0.035$ sample, in which the transport properties are dominated by the electron-like carriers. This suggests that if the nematicity is band selective, the electron-pockets play the major role.

Elasto-Nernst

Figure 3a, d shows the temperature dependence of the Nernst coefficient ν of the $x = 0$ and the $x = 0.035$ sample, respectively (see Supplementary Note 8 and Supplementary Fig. 10 for the magnetic-field dependence of the Nernst coefficient). First of all, one can notice that, differently from the Seebeck coefficient, ν is

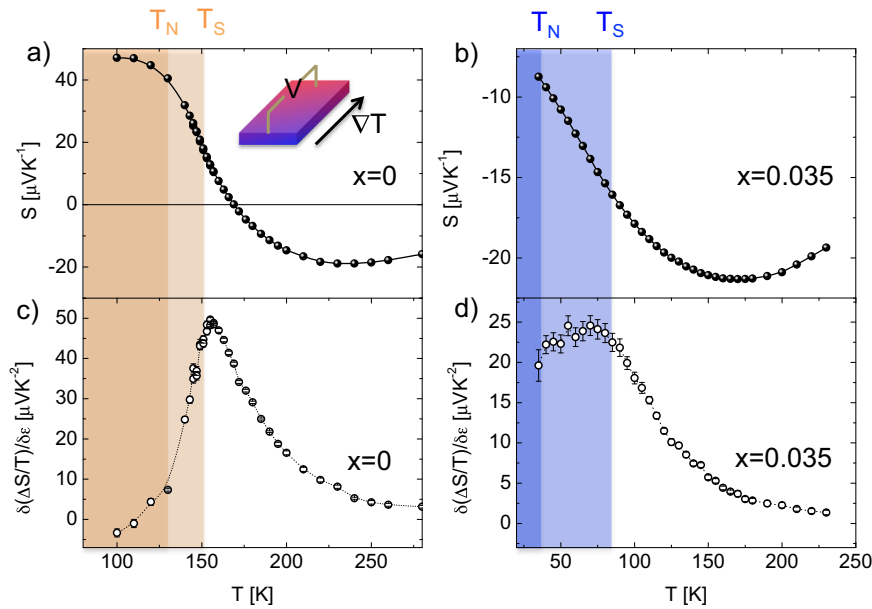


Fig. 2 Elasto-Seebeck effect of the $\text{LaFe}_{1-x}\text{Co}_x\text{AsO}$ compounds with $x = 0$ and $x = 0.035$. **a** Temperature dependence of the Seebeck coefficient S of the $\text{LaFe}_{1-x}\text{Co}_x\text{AsO}$ compounds with $x = 0$. **b** Temperature dependence of the strain derivative of the T -normalized Seebeck coefficient $\delta(\Delta S/T)/\delta\epsilon$ $x = 0$ compound. **c** Temperature dependence of the Seebeck coefficient S of the $\text{LaFe}_{1-x}\text{Co}_x\text{AsO}$ compounds with $x = 0.035$. **d** Temperature dependence of the strain derivative of the T -normalized Seebeck coefficient $\delta(\Delta S/T)/\delta\epsilon$ $x = 0.035$ compound. The dark-orange and the dark-blue areas indicate the regions where the long range structural and magnetic ordered states are both established. The error-bars represent the standard errors (see Supplementary Note 7, Supplementary Figs. 7–9).

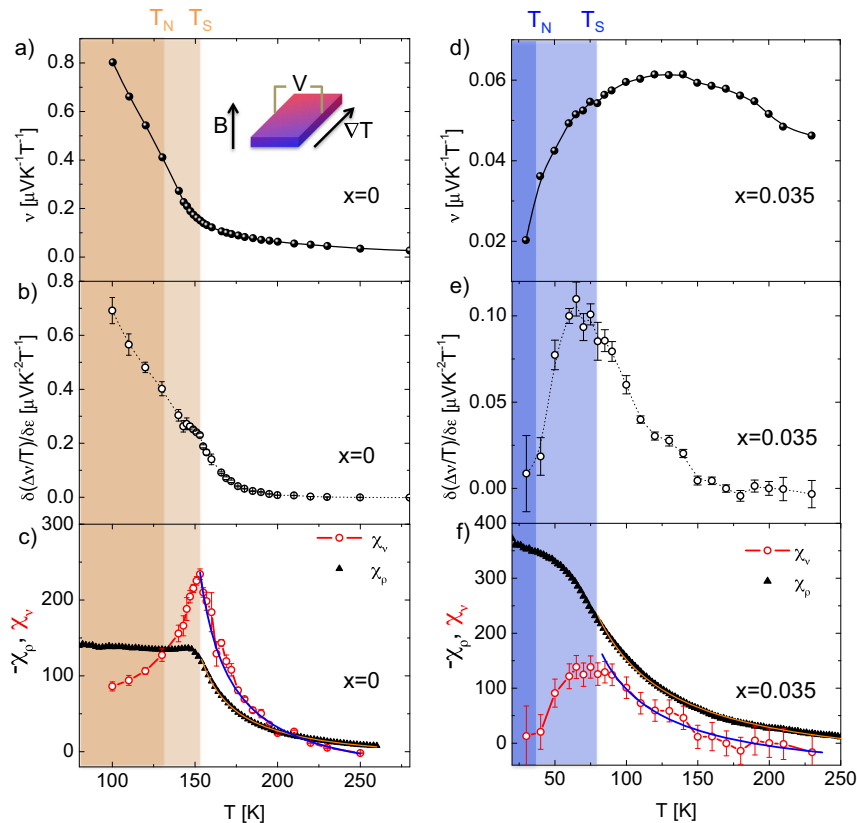


Fig. 3 Elasto-Nernst effect of the $\text{LaFe}_{1-x}\text{Co}_x\text{AsO}$ compounds with $x = 0$ and $x = 0.035$. **a** Temperature dependence of the Nernst coefficient v of the $x = 0$ compound. **b** Temperature dependence of the strain derivative of the T -normalized Nernst coefficient $\delta(\Delta v/T)/\delta\epsilon$ $x = 0$ compound. **c** Temperature dependence of the Nernst coefficient v of the $x = 0.035$ compound. **d** Temperature dependence of the strain derivative of the T -normalized Nernst coefficient $\delta(\Delta v/T)/\delta\epsilon$ $x = 0.035$ compound. **e** Temperature dependence of the Nernst coefficient v of the $x = 0.035$ compound. **f** Temperature dependence of the Nernst coefficient v of the $x = 0.035$ compound. The blue (orange) solid lines in fig. **c**, **f** represent the Curie–Weiss fit for $T > T_S$ of χ_v ($-\chi_p$). The dark-orange and the dark-blue areas indicate the regions where the long range structural and magnetic ordered states are both established. The error-bars represent the standard errors.

positive in the considered temperature range for both the compounds. Indeed, in the Nernst effect the contribution of different types of carriers is independent on the sign of their electric charge²³. Hence, the contributions by hole-like and electron-like pockets tends to sum up instead of compensating. This effect is also called ambipolar Nernst effect²³ and it is responsible for the violation of the Sondheimer's cancellation²⁴, which typically causes the suppression of the Nernst coefficient in single-band materials. In addition, in the parent compound, ν undergoes an abrupt increase at T_S , consistent with previous reports^{9,11}. This has been sometimes attributed to the Fermi surface distortion caused by the development of the long range magnetic ordering and the consequent band reorganisation with the appearance of Dirac-cone-like bands^{9,10}. In the $x=0.035$ compound the Nernst coefficient decreases in absolute value with respect to the parent compound. The reduction of ν upon Co-doping has been also observed in the 122 family, where it has been interpreted as the vanishing of the Dirac-cone effects due to the suppression of the magnetic order¹⁰. Furthermore, the electron doping causes also a tendency towards the domination of the electron-like carriers with the reduction of the ambipolar effect.

Figure 3b, e presents the temperature dependence of the strain derivative of the Nernst coefficient $\delta(\Delta\nu/T)/\delta\epsilon$ as a function of T , where $\Delta\nu = \nu(\epsilon) - \nu(\epsilon=0)$. In analogy to the strain derivative of the Seebeck effect, also $\delta(\Delta\nu/T)/\delta\epsilon$ presents a diverging behavior in the tetragonal phase and a change of regime at around T_S . Note, that these data alone do not allow to extract a clear information of the strain dependence of the Nernst coefficient as a function of doping, since the apparent strong reduction of $\delta(\Delta\nu/T)/\delta\epsilon$ from the $x=0$ to the $x=0.035$ compound is inevitably connected to the strong doping dependence of the Nernst coefficient ν itself as presented in Fig. 3a, d. In order to eliminate this particular cause of the amplitude variation, we normalize the strain dependences with respect to the unstrained ν and define a Nernst nematic susceptibility $\chi_\nu = \delta(\Delta\nu/\nu)/\delta\epsilon$. It is important to notice that the ambipolar nature of the Nernst effect prevents ν to cross the zero value in our compounds, in contrast to the Seebeck coefficient discussed above. χ_ν can be directly compared to the susceptibility calculated from the elastoresistivity $\chi_\rho = -\delta(\Delta\rho/\rho)/\delta\epsilon$ ²², whose value is generally assumed as the response of the electronic nematic order parameter to the applied strain^{5,6,22}. The result is presented in Fig. 3c, f for the $x=0$ and the $x=0.035$ sample, respectively.

For $T > T_S$, we checked the consistency of our data with a Curie–Weiss fit $\chi_\nu = \chi_0 + C/(T - T^*)$, where χ_0 is an intrinsic piezoelectric effect unrelated to the electronic nematicity, C is the Curie constant and T^* is the Curie temperature^{5,6}. In particular, T^* must be the same for χ_ν and χ_ρ , because it represents the mean

field electronic nematic critical temperature^{5,6}. Hence, for the fit, we fixed T^* to the value obtained by fitting χ_ρ ²² (orange lines in Fig. 3c, f), since it must be unvaried. In particular, $T^* = 134.5 \pm 8.0$ K and $T^* = 38.4 \pm 9.2$ K for the $x=0$ and the $x=0.035$ sample, respectively, while χ_0 and C have been left free to vary. The results are shown in Fig. 3c, f, where the blue lines represent the fitting curves, which nicely interpolate the experimental data. This confirms the Nernst effect as a primary probe for detecting and tracking the electronic nematic fluctuations.

Let's now focus on the absolute value of χ_ν and χ_ρ . Interestingly, χ_ν tends to decrease from $x=0$ to $x=0.035$, reaching the respective maximal value of around 230 and 120 close to T_S . On the contrary χ_ρ increases with doping. The increase of χ_ρ due to Co-doping in the $\text{Ba}(\text{Fe},\text{Co})_2\text{As}_2$ series was attributed to an increase of the nematic fluctuation intensity towards the optimally doped composition, which maximizes the superconducting critical temperature^{5,6}. By assuming that both χ_ν and χ_ρ should reflect the response of the nematic order parameter to the applied strain, the reason for their mismatch deserves some consideration. The Nernst coefficient is a complex quantity, which results from a nontrivial combination of the resistivity tensor ρ and the Peltier thermoelectric tensor α , reading $\nu = \alpha_{xy}\rho_{yy} - \alpha_{xx}\rho_{xy}$ ²⁵. In this notation x is the direction along which strain and heat gradient (or electric current) are applied, while y is the transverse direction. In complex materials, such as the iron-based superconductors, the experimental prediction of ν is usually unsuccessful due to the complications of the multiband nature. However, in the next section, we show that the behavior of the elasto-Nernst of the $x=0.035$ compound (closer to the single-band condition thanks to the doping) can be reasonably obtained from the other transport coefficients, in a self-consistent scenario (a partial analysis is also reported in Supplementary Note 4 and Supplementary Fig. 5 for the $x=0$ compound).

Analysis of the transport coefficients of the $x=0.035$ compound

First of all, in a single-band approximation, it is possible to evaluate also a Seebeck susceptibility $\chi_S = \delta(\Delta S/S)/\delta\epsilon$, shown in Fig. 4a as a function of T . For $T > T_S$, we interpolated the χ_S curve with a Curie–Weiss function, fixing again T^* to the value obtained by fitting χ_ρ . As in case of χ_ν , the Curie–Weiss curve nicely reproduces the experimental data. The Seebeck coefficient is explicated in terms of transport coefficients as $S = \alpha_{xx}\rho_{xx}$, where α_{xx} and ρ_{xx} are the diagonal terms of the Peltier and the resistivity tensors, respectively. It is immediate to verify that $\chi_S = \chi_\rho + \chi_\alpha$, where $\chi_\alpha = \delta(\Delta\alpha_{xx}/\alpha_{xx})/\delta\epsilon$. From these relations, one can evaluate the temperature dependence of α_{xx} and χ_α , presented in Fig. 4b. It must be noticed that χ_α is of the same order of magnitude as χ_ρ . However, they exhibit an opposite sign, which is understandable,

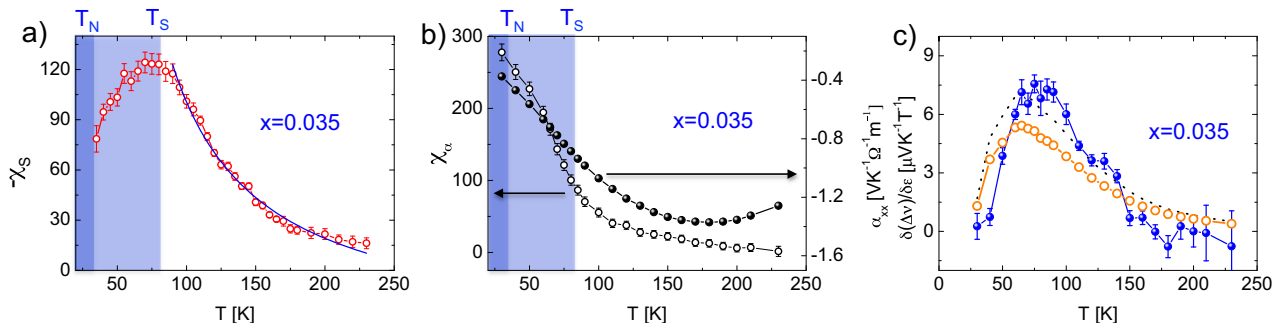


Fig. 4 Analysis of the transport coefficients of the $x=0.035$ compound. **a** Temperature dependence of $-\chi_S$ (red circles with solid line) for the $x=0.035$ compound. The blue solid line is the Curie–Weiss fit. **b** Temperature dependence of χ_α (empty circles with solid line) and α_{xx} (black circles with solid line) for the $x=0.035$ compound. **c** Temperature dependence of experimental $\delta(\Delta\nu)/\delta\epsilon$ (blue circles with blue solid line) and calculated $\delta(\Delta\nu)/\delta\epsilon$ (orange empty circles with solid line) for the $x=0.035$ compound. The black dotted line represents the calculated $\delta(\Delta\nu)/\delta\epsilon$ multiplied by a factor 1.2. The error-bars represent the standard errors.

considering that $\alpha_{xx} \sim d\sigma_{xx}/dE = -\rho_{xx}^{-1}d\rho_{xx}/dE$, where σ_{xx} is the electrical conductivity and E is the energy.

At this point, one can consider χ_v and verify whether it is experimentally obtainable by a combination of the other transport coefficients. In the limit of small strain, in which we operate, one can safely state that $\rho_{xx} \simeq \rho_{yy}$ and $\delta\rho_{yy}/\delta\epsilon = (1/Y_p)\delta\rho_{xx}/\delta\epsilon$, where Y_p is the Poisson ratio of the piezoelectric device. The off-diagonal terms do not directly contribute to the anisotropy¹⁹. Hence, we can evaluate $\delta(v)/\delta\epsilon = \alpha_{xy}\delta\rho_{yy}/\delta\epsilon - \rho_{xy}\delta\alpha_{xx}/\delta\epsilon$, where α_{xy} is obtained by combining the transport properties in unstrained conditions²⁵. The result is shown in Fig. 4c in comparison with the experimental value. The two curves are in good agreement, demonstrating experimentally the validity of the description of transport properties in terms of conductivity and Peltier tensors.

Several remarks are in order. First of all we point out that a self-consistent interconnection of transport coefficients is rarely proven experimentally. One might speculate that the clean result is facilitated by the use of strain derivatives, which render spurious effects less important. Second, our analysis shows the necessity of two different contributing transport coefficients (ρ_{xx} and α_{xx}) to explain the behavior of v under strain.

The validation of this method is an important result because it can be applied to the investigation of all the single-band systems in which the proximity to an instability or a phase transition renders electronic properties susceptible to the strain. This includes many cuprates superconductors and doped iron-based superconductors.

DISCUSSION

In the previous section, we demonstrated the existence of a finite χ_a beside a finite χ_ρ . With this established, one can conjecture on the microscopic mechanisms that determine the transport nematic phenomenology. From the transport point of view a large susceptibility to the applied strain is the result of a strong anisotropy either in the scattering time and/or in the Fermi surface parameters, such as the Fermi velocity. Generally, an anisotropic scattering time as a source for transport anisotropy is supported by a pure spin-nematic scenario^{26–29}, while the pure orbital-ordering description takes mainly into account anisotropies of the Fermi surface parameters^{30–33}.

The advantage of the thermoelectric properties and especially of the Nernst effect is their capability to catch both these aspects. This can be directly inferred from the simplest imaginable model for a single-band material. As mentioned above, from the solution of the Boltzmann equation, one can obtain the following link between the Peltier thermoelectric tensor and the conductivity tensor: $\mathbf{a} = (\pi^2/3)(k_B^2T/q)(d\sigma/dE)|_{E=E_F}$, with k_B the Boltzmann constant⁸. Hence, \mathbf{a} is a direct measurement of the variation in conductivity caused by a (even infinitesimal) shift in the chemical potential, induced, for instance, by a Fermi surface distortion. In particular, for the Nernst coefficient, assuming a smooth (but not null) variation of the mobility with respect to the energy, the following expression can be derived: $v = (\pi^2/3)(k_B^2T/e)\mu/E_F$, where the dependence on both the mobility and the Fermi energy appears explicitly⁸. Naturally, this expression cannot be quantitatively applied to complex materials like iron-based superconductors, but it is very useful to comprehend at a glance the versatility of the Nernst coefficient in probing the electronic properties of a material. Hence, assuming the nematicity in iron-based superconductors as an electron-originated effect, an impressive response of the thermoelectric properties to the strain is not completely surprising.

In the context of cuprate superconductors, it was explicitly predicted that the Nernst effect anisotropy is a very sensitive probe of Fermi surface distortions caused by electron-nematic order¹⁹. This is caused by a large anisotropy in \mathbf{a} , which overcomes the anisotropy of ρ and results particularly enhanced in

correspondence of a change of the Fermi surface topology¹⁹. This means that, if only an orbital anisotropy dominates the transport, a χ_a substantially larger than χ_ρ can be expected. Since in our case $|\chi_\rho| \geq |\chi_a|$, it is likely that a significant contribution from an anisotropic scattering time must be present.

On the other hand, it has been reported that the NMR spin-lattice relaxation rate $(T_1T)^{-1}$ of LaFeAsO is finite well above T_S , as a signature of persistent spin fluctuations³⁴. For $T < T_S$, $(T_1T)^{-1}$ increases a lot, before diverging in correspondence of T_N , where spin fluctuations freeze³⁴. Interestingly, neither χ_ρ nor χ_v seem to be sensitive to the magnetic transition (see magnetization data Supplementary Note 1 and Supplementary Fig. 2) and they do not follow the trend of $(T_1T)^{-1}$. This suggests that they are not mimicking the spin susceptibility of the system. As a consequence, the existence of an anisotropic scattering time, directly linked to anisotropic spin fluctuations, is not sufficient to explain the transport anisotropy, but an orbital contribution from the distortion of Fermi surface must be included. Hence, to shed light on the cryptic nematic phase of iron-based superconductors, it is evident that a theoretical picture, which includes different microscopic mechanism must be adopted. In this sense the orbital-selective spin-nematic model is a promising candidate, since it predicts that, once the orbital character of the spin fluctuations is taken into account, both the anisotropy in scattering rate and in the Fermi surface parameters (i.e., the Fermi velocities) must play a substantial role^{35–37}.

In summary, we measured the strain derivative of the Seebeck and the Nernst effect of two single crystals belonging to the 1111 family of iron-based superconductors. We observed that thermoelectric properties, in proximity of a nematic instability, are strongly susceptible to a vanishingly small strain. The inspection of the Seebeck effect provided a clear signature of the band-selective character of the nematic phenomenology in case of a multiband system, which is a fundamental information for the definition of a nematic order parameter. In addition, by defining a Nernst nematic susceptibility, we experimentally demonstrated that an anisotropy in the resistivity tensor ρ is not enough to explain the behavior of the thermoelectric properties, but a finite anisotropy in the Peltier-tensor \mathbf{a} must be included. This suggests that the transport nematic phenomenology is likely to be the result of the combined effect of both an anisotropic scattering time and Fermi surface distortions, pointing out that in a realistic description, beside the spin fluctuations also the orbital character is a fundamental ingredient. We expect that these results will trigger novel theoretical insights, setting new bounds for the anisotropic transport models and giving a substantial contribution to the understanding of the nematic puzzle.

METHODS

Crystal growth

The crystals were obtained using the solid-state single crystal growth method at ambient pressure using Na–As as a liquid phase promoting an abnormal grain growth due to enhanced interfacial anisotropy by introducing a liquid–solid interface. This is a different strategy from the usually used flux growth. As this growth is based on polycrystalline starting materials, a polycrystalline sample of LaFeAsO was prepared using a two-step solid-state reaction. The obtained polycrystalline pellets and Na–As powder were layered into an alumina crucible. The molar ratio of LaFeAsO to Na–As used was 1:4, which corresponds to a ratio in volume of about 1:1. The material was heated to 1080 °C and annealed for 200 h. By using this method single crystals sized up to $2 \times 3 \times 0.4$ mm³ were obtained (see Supplementary Fig. 1). Reference¹⁷ gives a detailed description of the synthesis process of all the investigated compounds. The crystals were analyzed using SEM with EDX, Laue backscattering, powder X-ray diffraction and SQUID magnetometry measurements (see Supplementary Note 1 and Supplementary Fig. 2). In addition, preliminary resistivity and Hall effect measurements have been performed (see Supplementary Note 2, Supplementary Fig. 3).

Elasto-thermoelectric transport measurements

We applied an in-plane uniaxial strain by gluing the samples on the surface of a commercial piezoelectric stacks (Part. No. Pst 150/5 × 5 × 7, form Piezomechanik, Munich, Germany), using the Devcon General Purpose Adhesive Epoxy (No. 14250). The as-grown-single crystals have been cleaved with a thin blade down to a thickness of about 30–40 μm in order to be sure that the strain is fully transferred across the sample²². The final dimensions of the samples were typically 1 × 1 × 0.04 mm³. The samples have been glued oriented, in order to align the straining axis of the piezo to the orthorhombic axis of our compounds, corresponding to the [110] crystalline direction, along which the nematic fluctuations are expected to develop^{5,6,22}. Following the same procedure adopted in the elasto-resistivity experiments^{5,6,22}, the applied strain has been measured by using a resistive strain gauge mounted on the back side of the piezo-stack and read through a Wheatstone bridge. The temperature evolution of the applied strain and the Poisson ratio of the piezo-stack have been characterized (see Supplementary Notes 5 and 6 and Supplementary Fig. 6). Thanks to the homogeneity of the piezo-stack, if the sample is thin enough (as in our case) the reading of the gauge nicely correspond to the strain applied to the sample^{5,22}. In order to perform the thermoelectric characterization, we built a thermal circuit by connecting one side of the sample to a resistive heater ($R = 2.7$ kΩ) and the other side to the thermal mass of our sample holder. The thermal connections have been made by using silver wires glued with a thermal epoxy (Wakefield-Vette Delta Bond 152-KA). The temperature gradient has been measured using a Chromel-Au-Chromel differential thermocouple, calibrated in magnetic field. Longitudinal and transverse couples of electrodes have been attached to the sample to pick up the Seebeck and the Nernst signals (Fig. 1a). The electrical leads have been realized by gluing 50-μm-thick silver wires to the sample with a silver paste (Dupont 4929N). Figure 1b, e shows the measurement procedure for collecting the strain derivative of the Seebeck and the Nernst coefficients. First of all the sample, mounted on the piezo, is thermalized at the desired temperature T and in case of the Nernst coefficient measurement a constant magnetic-field \mathbf{B} is applied with a direction perpendicular to the ab -plane of the sample. Then, a heating power W_H is applied through the heater to the sample (bottom panels in Fig. 1c, e) in order to create a temperature gradient $\nabla T = \Delta T/l_T$, where ΔT is the temperature difference measured by the thermocouple and l_T is the distance between the thermocouple tips. This causes a response in the Seebeck and Nernst voltages (ΔV_S and ΔV_N in the top panels of Fig. 1b, e). The corresponding Seebeck and Nernst coefficients are $S = -\Delta V_S/(I_S \nabla T)$ and $N = \Delta V_N/(I_N \nabla T)$, where I_S and I_N are the distance between the respective couples of electrodes. Then, the piezo actuator is activated and the applied voltage is varied along the cycle $0 \text{ V} \rightarrow 100 \text{ V} \rightarrow -30 \text{ V} \rightarrow 0 \text{ V}$. During this process, we measure simultaneously the variation of the Seebeck (Nernst) coefficient ΔS (ΔN) with the corresponding electrodes and the effective strain ϵ with the strain gauge (middle panels in Fig. 1b, e). In the regime of small strain ($\epsilon < 0.1\%$) in which we operate ΔS and ΔN are linearly dependent on ϵ (Fig. 1c, f). Hence, we can extract $\delta(\Delta S)/\delta\epsilon$ or $\delta(\Delta N)/\delta\epsilon$ as the angular coefficient of the linear fit in the ΔS or ΔN vs ϵ graph (red lines in Fig. 1c, f). In addition for the Nernst coefficient we antisymmetrized the signal by inverting the magnetic-field \mathbf{B} in order eliminate any spurious contribution.

By repeating this procedure for all the required temperatures we can track the T dependence of the elasto-Seebeck and elasto-Nernst effects.

DATA AVAILABILITY

The data that support the findings of this study are available from the corresponding author upon reasonable request.

Received: 31 August 2020; Accepted: 3 February 2021;

Published online: 17 March 2021

REFERENCES

- Daou, R. et al. Broken rotational symmetry in the pseudogap phase of a high- T_c superconductor. *Nature* **463**, 519–522 (2010).
- Lawler, M. J. et al. Intra-unit-cell electronic nematicity of the high- T_c copper-oxide pseudogap states. *Nature* **466**, 347–351 (2010).
- Fernandes, R. M., Chubukov, A. V. & Schmalian, J. What drives nematic order in iron-based superconductors? *Nat. Phys.* **10**, 97–104 (2014).
- Chuang, T.-M. et al. Nematic electronic structure in the “parent” state of the iron-based superconductor $\text{Ca}(\text{Fe}_{1-x}\text{Co}_x)_2\text{As}_2$. *Science* **327**, 181–184 (2010).
- Chu, J.-H., Kuo, H.-H., Analytis, J. G. & Fisher, I. R. Divergent nematic susceptibility in an iron arsenide superconductor. *Science* **337**, 710–712 (2012).
- Kuo, H.-H., Chu, J.-H., Palmstrom, J. C., Kivelson, S. A. & Fisher, I. R. Ubiquitous signatures of nematic quantum criticality in optimally doped Fe-based superconductors. *Science* **352**, 958–962 (2016).
- Hosoi, S. et al. Nematic quantum critical point without magnetism in FeSe $_{1-x}\text{S}_x$ superconductors. *Proc. Natl. Acad. Sci. USA* **113**, 8139–8143 (2016).
- Behnia, K. The Nernst effect and the boundaries of the Fermi liquid picture. *J. Phys. Condens. Matter* **21**, 113101 (2009).
- Pallecchi, I., Caglieris, F. & Putti, M. Thermoelectric properties of iron-based superconductors and parent compounds. *Supercond. Sci. Technol.* **29**, 073002 (2016).
- Matusiak, M., Bukowski, Z. & Karpinski, J. Doping dependence of the Nernst effect in $\text{Eu}(\text{Fe}_{1-x}\text{Co}_x)_2\text{As}_2$: Departure from Dirac-Fermion physics. *Phys. Rev. B* **83**, 224505 (2011).
- Kondrat, A., Behr, G., Büchner, B. & Hess, C. Unusual Nernst effect and spin density wave precursors in superconducting $\text{LaFeAsO}_{1-x}\text{F}_x$. *Phys. Rev. B* **83**, 092507 (2011).
- Behnia, K. & Aubin, H. Nernst effect in metals and superconductors: a review of concepts and experiments. *Rep. Prog. Phys.* **79**, 046502 (2016).
- Fujii, T., Shirachi, T. & Asamitsu, A. Measurement of the thermopower anisotropy in iron arsenide. *Phys. C* **530**, 31–34 (2016).
- Jiang, S., Jeevan, H. S., Dong, J. & Gegenwart, P. Thermopower as a sensitive probe of electronic nematicity in iron pnictides. *Phys. Rev. Lett.* **110**, 067001 (2013).
- Matusiak, M., Babji, M. & Wolf, T. Anisotropy of the Seebeck and Nernst coefficients in parent compounds of the iron-based superconductors. *Phys. Rev. B* **97**, 100506 (2018).
- Matusiak, M., Rogacki, K. & Wolf, T. Thermoelectric anisotropy in the iron-based superconductor $\text{Ba}(\text{Fe}_{1-x}\text{Co}_x)_2\text{As}_2$. *Phys. Rev. B* **97**, 220501 (2018).
- Kappenberger, R. et al. Solid state single crystal growth of three-dimensional faceted LaFeAsO crystals. *J. Cryst. Growth* **483**, 9–15 (2018).
- Wang, L. et al. Nematicity and structure in $\text{LaFe}_{1-x}\text{Co}_x\text{AsO}$. *J. Magn. Magn. Mater.* **482**, 50–53 (2019).
- Hackl, A. & Vojta, M. Nernst-effect anisotropy as a sensitive probe of Fermi-surface distortions from electron-nematic order. *Phys. Rev. B* **80**, 220514 (2009).
- Wang, C. et al. Effects of cobalt doping and phase diagrams of $\text{LaFe}_{1-x}\text{Co}_x\text{AsO}$ ($l = \text{La}$ and Sm). *Phys. Rev. B* **79**, 054521 (2009).
- Okram, G. S., Kaurav, N., Soni, A., Pal, A. & Awana, V. P. S. Effect of co-doping on the resistivity and thermopower of $\text{SmFe}_{1-x}\text{Co}_x\text{AsO}$ ($0.0 \leq x \leq 0.3$). *AIP Adv.* **2**, 042137 (2012).
- Hong, X. et al. Evolution of the nematic susceptibility in $\text{LaFe}_{1-x}\text{Co}_x\text{AsO}$. *Phys. Rev. Lett.* **125**, 067001 (2020).
- Bel, R., Behnia, K. & Berger, H. Ambipolar Nernst effect in NbSe_2 . *Phys. Rev. Lett.* **91**, 066602 (2003).
- Sondheimer, E. H. & Wilson, A. H. The theory of the galvanomagnetic and thermomagnetic effects in metals. *Proc. R. Soc. A* **193**, 484–512 (1948).
- Meinero, M. et al. Unusual thermoelectric properties of BaFe_2As_2 in high magnetic fields. *Phys. Rev. B* **98**, 155116 (2018).
- Fernandes, R. M., Abrahams, E. & Schmalian, J. Anisotropic in-plane resistivity in the nematic phase of the iron pnictides. *Phys. Rev. Lett.* **107**, 217002 (2011).
- Fernandes, R. M. et al. Effects of nematic fluctuations on the elastic properties of iron arsenide superconductors. *Phys. Rev. Lett.* **105**, 157003 (2010).
- Breitkreiz, M., Brydon, P. M. R. & Timm, C. Resistive anisotropy due to spin-fluctuation scattering in the nematic phase of iron pnictides. *Phys. Rev. B* **90**, 121104 (2014).
- Gastiasoro, M. N., Paul, I., Wang, Y., Hirschfeld, P. J. & Andersen, B. M. Emergent defect states as a source of resistivity anisotropy in the nematic phase of iron pnictides. *Phys. Rev. Lett.* **113**, 127001 (2014).
- Kontani, H., Saito, T. & Onari, S. Origin of orthorhombic transition, magnetic transition, and shear-modulus softening in iron pnictide superconductors: Analysis based on the orbital fluctuations theory. *Phys. Rev. B* **84**, 024528 (2011).
- Lee, C.-C., Yin, W.-G. & Ku, W. Ferro-orbital order and strong magnetic anisotropy in the parent compounds of iron-pnictide superconductors. *Phys. Rev. Lett.* **103**, 267001 (2009).
- Valenzuela, B., Bascones, E. & Calderón, M. J. Conductivity anisotropy in the antiferromagnetic state of iron pnictides. *Phys. Rev. Lett.* **105**, 207202 (2010).
- Chen, C.-C. et al. Orbital order and spontaneous orthorhombicity in iron pnictides. *Phys. Rev. B* **82**, 100504 (2010).
- Ok, J. M. et al. Nematicity and magnetism in LaFeAsO single crystals probed by ^{75}As nuclear magnetic resonance. *Phys. Rev. B* **97**, 180405 (2018).
- Fanfarillo, L., Benfatto, L. & Valenzuela, B. Orbital mismatch boosting nematic instability in iron-based superconductors. *Phys. Rev. B* **97**, 121109 (2018).

36. Fernández-Martín, R., Fanfarillo, L., Benfatto, L. & Valenzuela, B. Anisotropy of the dc conductivity due to orbital-selective spin fluctuations in the nematic phase of iron superconductors. *Phys. Rev. B* **99**, 155117 (2019).
37. Fanfarillo, L. et al. Orbital-dependent fermi surface shrinking as a fingerprint of nematicity in FeSe. *Phys. Rev. B* **94**, 155138 (2016).

ACKNOWLEDGEMENTS

We thank R. Wachtel, D. Meiler, J. Werner, L. Giebeler, S. Müller-Litvanyi, and S. Gass (all IFW Dresden) for support. FC thanks Laura Fanfarillo for valuable scientific discussion. This work has been supported by the Deutsche Forschungsgemeinschaft (DFG) through the Priority Programme SPP1458 (Grant No. BU887/15-1), under grant DFG-GRK1621, and through the Emmy Noether Programme WU595/3-3 (S.W.). This project has been supported by the Deutsche Forschungsgemeinschaft through the Research Projects CA 1931/1-1 (F.C.) and AS 523/3-1 (S.A.). This project has received funding from the European Research Council (ERC) under the European Unions' Horizon 2020 research and innovation programme (grant agreement No 647276–MARS–ERC-2014-CoG).

AUTHOR CONTRIBUTIONS

F.C., C.W., and X.C.H. performed the measurements and the data analysis. S.S. contribute to the data interpretation. R.K., S.A., and S.W. grew and characterized the samples. F.C., B.B., and C.H. designed and supervised the project. F.C. and C.H. wrote the manuscript.

FUNDING

Open Access funding enabled and organized by Projekt DEAL.

COMPETING INTERESTS

The authors declare no competing interests.

ADDITIONAL INFORMATION

Supplementary information The online version contains supplementary material available at <https://doi.org/10.1038/s41535-021-00324-7>.

Correspondence and requests for materials should be addressed to F.C.

Reprints and permission information is available at <http://www.nature.com/reprints>

Publisher's note Springer Nature remains neutral with regard to jurisdictional claims in published maps and institutional affiliations.



Open Access This article is licensed under a Creative Commons Attribution 4.0 International License, which permits use, sharing, adaptation, distribution and reproduction in any medium or format, as long as you give appropriate credit to the original author(s) and the source, provide a link to the Creative Commons license, and indicate if changes were made. The images or other third party material in this article are included in the article's Creative Commons license, unless indicated otherwise in a credit line to the material. If material is not included in the article's Creative Commons license and your intended use is not permitted by statutory regulation or exceeds the permitted use, you will need to obtain permission directly from the copyright holder. To view a copy of this license, visit <http://creativecommons.org/licenses/by/4.0/>.

© The Author(s) 2021